SEASONAL DEPENDENCE OF GEOMETRICAL AND OPTICAL PROPERTIES OF TROPICAL CIRRUS DETERMINED FROM LIDAR, RADIOSONDE, AND SATELLITE OBSERVATIONS OVER THE TROPICAL INDIAN OCEAN (MALDIVES)

Patric Seifert[1], Albert Ansmann[1], Dietrich Althausen[1], Ulla Wandinger[1], Andrew J. Heymsfield[2], Steven T. Massie[2]

[1] *Leibniz Institute for Tropospheric Research, Permoserstr. 15, D-04318 Leipzig, Germany, E-mail: seifert@tropos.de, albert@tropos.de, dietrich@tropos.de, ulla@tropos.de*
[2] *National Center for Atmospheric Research, P.O. Box 3000, Boulder, CO 80307-3000, USA, E-mail: heyms1@ucar.edu, massie@ucar.edu*

ABSTRACT

Cirrus clouds detected with a six-wavelength aerosol lidar in the tropical region of the Maldives (4.1° N, 73.3° E) were characterized in terms of seasonal geometrical, optical, and thermal properties. The dataset was collected during the Indian Ocean Experiment between February 1999 and March 2000, covering two seasons of the northeast monsoon and one of the southwest monsoon. Cirrus visible optical depth, mean extinction coefficient, and lidar ratio were derived from the 532-nm elastic-backscatter lidar signals. Temperature information from radiosondes launched frequently at the lidar site was used to characterize the thermal structure of the tropical troposphere and the temperature dependence of the optical and geometrical cirrus properties. The analysis of satellite-derived outgoing longwave radiation data showed that the occurrence of cirrus is highly correlated with deep convection. Cirrus clouds were detected at 50% of the measurement time with an average mid-cloud height of 12.6 km. 18% of the analyzed clouds were subvisible, 52% were thin cirrus, and 30% were cirrostratus.

1. INTRODUCTION

20% to 35% of the globe are regularly covered with cirrus [1],[2]. The highest rates of coverage can be found in the area of the intertropical convergence zone (ITCZ) with an average value of 45% [2]. Such values lead to a significant impact of cirrus clouds on local meteorological processes as well as on the global heat budget of the atmosphere [1],[2]. Several field campaigns were carried out in various regions of the globe to improve the knowledge on the climate impact of cirrus clouds. But especially in the tropics vertically and temporally highly resolved measurements of cirrus cloud properties are still scarcely available.

This work presents the first long-term lidar-derived cirrus cloud statistics and information about cirrus cloud optical properties of the region of the tropical Indian Ocean. In the scope of the Indian Ocean Experiment (INDOEX) the transportable lidar system of the Leibniz Institute for Tropospheric Research (IFT, Leipzig, Germany) performed more than 30,000 minutes of multi-wavelength backscatter, extinction, and depolarization profiling at Hulule, Maldives (4.1° N, 73.3° E). Four individual field campaigns have been carried out in February/March 1999, July 1999, October 1999, and March 2000 so that the underlying dataset covers both, two seasons of the dry northeast (NE) monsoon (February/March 1999 and March 2000) as well as one season of the rainy southwest (SW) monsoon (July and October 1999). Section 2 summarizes the instrumentation of the experiment. Results are presented in Section 3.

2. INSTRUMENTATION

The optical data used in this work was recorded by the containerized multi-wavelength aerosol lidar, developed and operated by the IFT. A detailed description of the system can be found in [3].

Two Nd:YAG and two dye lasers simultaneously emit pulses at 355, 400, 532, 710 (parallel polarized), 800, and 1064 nm with a repetition rate of 30 Hz. A scanning unit outside of the container, realized by a steerable mirror, permits measurements at zenith angles from $-90°$ to $90°$. A 0.53-m Cassegrain telescope collects the backscattered light. In addition to the elastic signals of the six emitted wavelengths, the inelastically scattered Raman signals of nitrogen at 387 nm (355 nm primary wavelength) and 607 nm (532 nm primary wavelength) as well as of water vapor at 660 nm (532 nm primary wavelength) are detected. A detection of Raman signals throughout

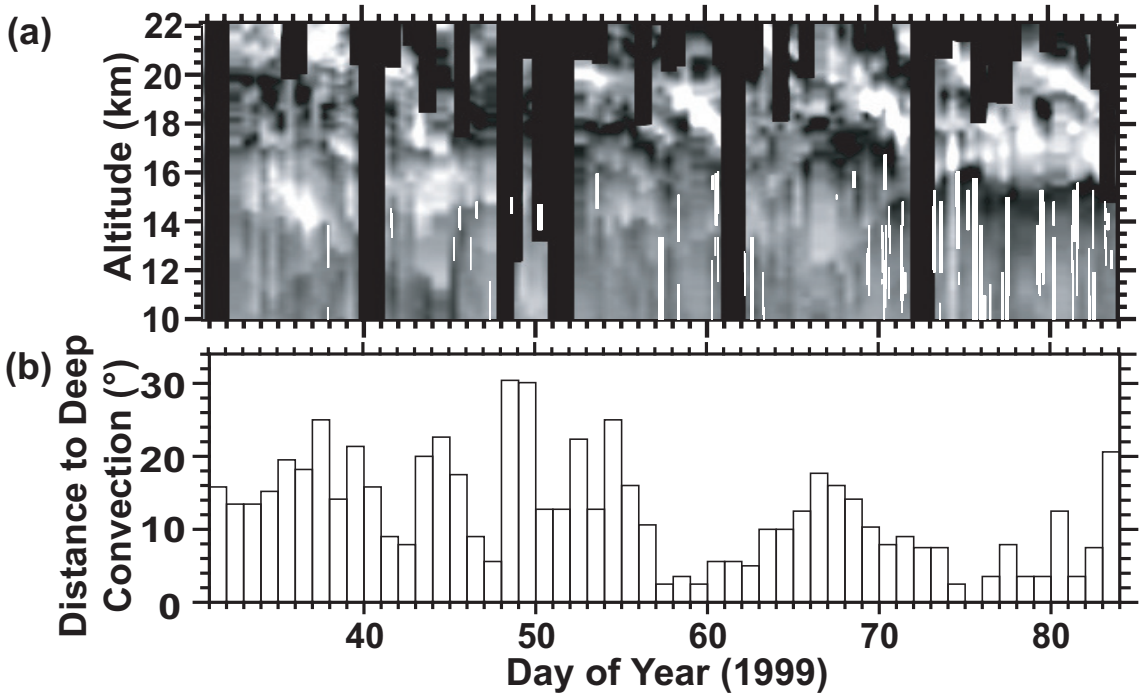

Fig. 1: (a) Temperature deviation from the average temperature of all radiosondes launched during Feb/Mar 1999. Black areas represent negative temperature deviations <–4 K, white areas represent positive temperature deviations >+4 K. Descending stratospheric waves are visible. White vertical lines: observed cirrus. (b) Distance between Hulule and nearest location with deep convection (OLR < 170 Wm^{-2}, $1° \approx 110$ km).

the troposphere is only possible at night when the background signal is negligible. The 710-nm signal is split up into a parallel (co-) and a perpendicular (cross-) polarized channel. Photomultipliers amplify the signal of the detected photons. The amplified signals are acquired either in analog (400, 532, 710, 800, 1064 nm) or in photon-counting mode (355, 387, 532, 607, 660 nm).

During the four field campaigns 250 radiosondes of the type Vaisala RS-80 were launched, providing vertical profiles of pressure, temperature, and humidity.

Satellite-derived outgoing longwave radiation (OLR) data of the Climate Diagnostics Center (CDC) [4] on a daily basis was used to obtain an overview of the distribution of convective activity in the region of the Maldives. OLR values less than approximately 170 Wm^{-2} indicate deep convection that is known to be a primary source of cirrus clouds in the tropics.

4. RESULTS

4.1 Temporal and Seasonal Distribution of cirrus clouds

During the NE-monsoon field campaigns the occurrence of cirrus clouds showed significant temporal variations. This is shown in Fig. 1 (a) where the temperature deviation field for the campaign of February/March 1999 is presented. White vertical lines indicate the occurrence of cirrus clouds. The temperature deviation was calculated from the average temperature of all radiosonde ascends in the respective time period (approximately two per day). White and black areas represent positive temperature deviations of more than +4 K and negative deviations of less than –4 K, respectively. Stratospheric wave characteristics are visible in Fig. 1 (a). They were identified as eastward propagating Kelvin waves in [5]. The cold phases of these waves (dark areas) are supposed to play a major role in the formation of upper-tropospheric cirrus clouds.

In Fig. 1 (a) four of these waves can be seen. Between day 30 and day 50 the upper troposphere was relatively warm and only few cirrus clouds were observed. When cold perturbations occurred at altitudes below 16 km, as between day 55 and 62 and day 69 and 84, also a high frequency of cirrus clouds was observed. However, an unambiguous relationship between the stratospheric waves and the cold perturbations and thus cirrus formation is not clearly recognizable from Fig. 1 (a). More significant correlations exist between the occurrence of cirrus clouds and the distance of the observation site to deep convection. Fig. 1 (b) presents the distance between Hulule and the nearest location with deep convection (in geographical degrees). It was calculated from the CDC

Tab. 2: Mean values and standard deviations (in parentheses) of geometrical and thermal cloud properties. The values are given for all observed cirrus cases as well as for the northeast monsoon and the southwest monsoon.

	All Cases		NE Monsoon		SW Monsoon	
Analyzed cases	193		114		79	
Cloud Base Height (km)	11.6	(1.9)	11.8	(1.9)	11.3	(2.0)
Cloud Top Height (km)	13.5	(1.5)	13.5	(1.6)	13.5	(1.5)
Cloud Depth (km)	1.9	(1.1)	1.6	(0.9)	2.2	(1.3)
Mid-Cloud Height (km)	12.6	(1.6)	12.7	(1.6)	12.4	(1.6)
Cloud Base Temperature (°C)	–48	(15)	–49	(15)	–46	(15)
Cloud Top Temperature (°C)	–63	(12)	–63	(12)	–62	(12)
Mid-Cloud Temperature (°C)	–56	(13)	–56	(13)	–54	(13)

OLR dataset. When deep convection was apparent in the vicinity of the Maldives also a high frequency of cirrus clouds was observed. This can especially be seen between day 57 and 62 and between day 69 and 84. The results presented in Fig. 1 suggest a relation between deep convection, stratospheric waves and the formation of cirrus clouds. Further analysis may be needed to solve this issue.

The lidar data collected during the four field campaigns were separated into the two monsoon seasons. Thus the data of February/March 1999 and March 2000 yield to the NE-monsoon dataset. The data of July and October 1999 provide the basis for the SW-monsoon dataset. Information about the occurrence frequency of cirrus clouds during the respective seasons is shown in Tab. 1. The summation of the results of both seasons yields a total of 193 cirrus cases and a total occurrence time of 14883 minutes out of a total measurement time of 30050 minutes. This corresponds to a total cirrus cloud frequency of 50%.

Tab. 1: Seasonal distribution of cirrus cases and cirrus occurrence time.

	NE Monsoon	SW Monsoon
No. of meas. min.	20761	9289
Cirrus cases	114	79
Cirrus detected (min)	8472	6411
Cirrus detected (%)	41	69

4.2 Cirrus Geometrical Properties

Cirrus geometrical properties such as cloud top and base were derived from the lidar signal at 532 nm wavelength. Because of a strong gradient of the lidar signal the cloud boundaries were easy to determine. For ascending and descending clouds the uppermost and lowermost boundaries were taken as cloud top and cloud base, respectively. All clouds above 7 km that were transparent for the lidar signal were included into the statistics. Even a thin water cloud at such altitudes attenuated the light much stronger than ice clouds did.

Tab. 2 provides an overview of the seasonal mean values of height and temperature of the cloud boundaries and of the cloud depth. Standard deviations are given in parentheses behind the mean values. Mid-cloud values for height and temperature are given as additional information. The values for the different seasons all vary marginally within the respective ranges of standard deviation. Only the cloud depth shows a considerable seasonal variation. With a mean depth of 1.6 km clouds during the NE monsoon were on average about 0.6 km thinner than during the SW monsoon.

4.3 Cirrus Optical Properties

The optical cirrus properties were derived from the 532-nm elastically backscattered lidar signal applying the Klett method [6],[7]. The Klett method allows one to calculate the vertical profile of the particle backscatter coefficient β_p of the cirrus cloud and the mean cloud extinction coefficient α, but requires the assumption of a specific extinction-to-backscatter (lidar-) ratio S. Assuming particle-free conditions above and below the cloud, S can be determined by setting $\beta_\mathrm{p} = 0$ in that region and varying the lidar ratio until $\beta_\mathrm{p} = 0$ on the opposite site of the cloud. Integration of α over the cloud depth yields the cloud optical depth τ.

An overview of the seasonal mean values of the optical cirrus properties is given in Tab. 3. The cloud types were classified after [8]. Significant seasonal differences are obvious from the frequency of the three cloud types. While during the convectively active SW monsoon 47% cirrostratus was detected it was only 20% during the NE monsoon. In turn, only 5% subvisible cirrus was observed during the SW monsoon, compared to 24% during the NE monsoon. Optical depth, extinction coefficient, and lidar ratio do not vary significantly between the different seasons.

The temperature dependence of the extinction coefficient α determined from all analyzed cirrus cases is illustrated in Fig. 2. As presented in [9] the distribu-

Tab. 3: Seasonal frequency, mean optical depth $\bar{\tau}$, mean extinction coefficient $\bar{\alpha}$, and mean lidar ratio $\bar{S}$ of subvisible cirrus, thin cirrus, and cirrostratus. Standard deviations of the mean values are given in parentheses. The cloud types are classified after [8].

	Subvisible Ci $\tau < 0.03$	Thin Cirrus $0.03 < \tau < 0.3$	Cirrostratus $\tau > 0.3$
All Cases			
Frequency	18%	52%	30%
$\bar{\tau}$	0.015 (0.008)	0.13 (0.08)	0.64 (0.30)
$\bar{\alpha}$ (km^{-1})	0.012 (0.009)	0.06 (0.03)	0.21 (0.11)
$\bar{S}$ (sr)	21 (3)	21 (7)	18 (3)
NE Monsoon			
Frequency	24%	56%	20%
$\bar{\tau}$	0.014 (0.008)	0.13 (0.07)	0.57 (0.22)
$\bar{\alpha}$ (km^{-1})	0.013 (0.009)	0.07 (0.03)	0.22 (0.10)
$\bar{S}$ (sr)	20 (3)	22 (6)	19 (2)
SW Monsoon			
Frequency	5%	48%	47%
$\bar{\tau}$	0.014 (0.003)	0.14 (0.08)	0.68 (0.33)
$\bar{\alpha}$ (km^{-1})	0.010 (0.005)	0.05 (0.03)	0.20 (0.12)
$\bar{S}$ (sr)	23 (3)	19 (7)	18 (4)

tion was fitted by a second-order polynomial function of the form $\alpha(T) = A_0 + A_1 T + A_2 T^2$. The coefficients are:
$A_0 = 5.683 \times 10^{-4}$
$A_1 = 1.375 \times 10^{-5}$
$A_2 = 8.833 \times 10^{-8}$.

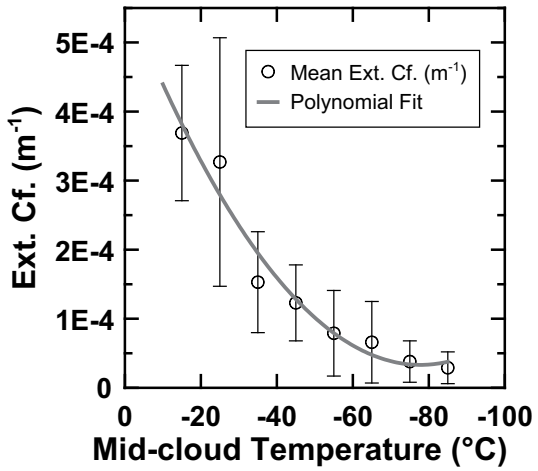

Fig. 2: Temperature dependence of extinction coefficient (Ext. Cf.) to mid-cloud temperature. The gray curve shows a polynomial fit of second order.

REFERENCES

1. Liou K. N. Influence of cirrus clouds on weather and climate processes: A global perspective, *Monthly Weather Review*, Vol. 114, 1167–1199, 1986.

2. Wylie D. P., et al. Four years of global cirrus cloud statistics using HIRS, *Journal of Climate*, Vol. 7, 1972–1986, 1994.

3. Althausen D. et. al. Scanning 6-wavelength 11-channel aerosol lidar, *Journal of Atmospheric and Oceanic Technology*, Vol. 17, 1469–1482, 2000.

4. Liebmann B. and Smith C. A. Description of a complete (interpolated) outgoing longwave radiation dataset, *Bulletin of the American Meteorological Society*, Vol. 77, 1275–1277, 1996.

5. Boehm M. T. and Verlinde J. Stratospheric influence on upper tropospheric tropical cirrus, *Geophysical Research Letters*, Vol. 27, 3209–3212, 2000.

6. Klett J. D. Stable analytical solution for processing lidar returns, *Applied Optics*, Vol. 20, 211–220, 1981.

7. Fernald F. G. Analysis of atmospheric lidar observations: some comments, *Applied Optics*, Vol. 23, 652–653, 1984.

8. Sassen K. and Cho B. S. Subvisual thin cirrus lidar data set for satellite verification and climatological research, *Journal of Applied Meterology*, Vol. 31, 1275–1285, 1992.

9. Sunilkumar S. V. and Parameswaran K. Temperature dependence of tropical cirrus properties and radiative effects, *Journal of Geophysical Research*, Vol. 110, D13205, 2005.